

Multisite observations of surface structures on AB Doradus in 1994 November

A. Collier Cameron,¹ F. M. Walter,² O. Vilhu,³ T. Böhm,⁴ C. Catala,⁴ S. Char,⁵
F. J. Clarke,¹ P. Felenbok,⁶ B. H. Foing,⁷ K. K. Ghosh,⁸ J. Hao,⁹ L. Huang,⁹ D. A.
Jackson,¹ E. Janot-Pacheco,¹⁰ S. Jiang,⁹ A.-M. Lagrange,¹¹ N. Suntzeff¹² and D. S. Zhai⁹

¹*School of Physics and Astronomy, University of St Andrews, North Haugh, St Andrews KY16 9SS*

²*SUNY, Stony Brook, Department of Earth and Space Sciences, Stony Brook, NY 11794, USA*

³*Observatory and Astrophysics Laboratory, University of Helsinki, SF-00014 Helsinki, Finland*

⁴*Observatoire Midi-Pyrenees, 14, Avenue Edouard Belin, 31400 Toulouse, France*

⁵*Department of Physics, University of La Serena, La Serena, Chile*

⁶*Observatoire de Paris, Section Meudon, F-92125 Meudon, France*

⁷*Solar System Division, ESA Space Science Department, ESTEC (SO), Postbus 299, 2200 AG Noordwijk, the Netherlands*

⁸*Vainu Bappu Observatory, Indian Institute of Astrophysics, Kavalur, Alangayam, TN 635701, India*

⁹*Beijing Astronomical Observatory, Chinese Academy of Sciences, Beijing 10080, China*

¹⁰*Departamento de Astronomia, Instituto Astronomico e Geofisico da USP, C. Postal 9638, 01065-970 Sao Paulo, Brazil*

¹¹*Lab. d'Astrophysique de Grenoble, UJF, BP53X F, 38041 Grenoble Cedex, France*

¹²*AURA Inc., Cerro Tololo Inter-American Observatory, La Serena, Chile*

Accepted 1999 April 8. Received 1999 March 31; in original form 1997 December 30

ABSTRACT

We present time-resolved optical spectroscopy and broad-band photometry of the rapidly rotating southern K0 dwarf star AB Doradus, obtained during 1994 November. The data were obtained as part of a collaboration dedicated to MULTI-SITE CONTINUOUS SPECTROSCOPY (MUSICOS), and entailed coordinated observations on three continents to obtain the fullest phase coverage possible subject to limitations of local weather conditions. The Doppler images from the three consecutive nights of the run show excellent mutual agreement, with a dark polar cap and numerous intermediate- and low-latitude features. Simultaneous optical photometry showed numerous short-duration *U*-band flares, and two longer duration optical flares with durations of the order of hours. The latter produced broad-band continuum enhancements throughout the optical spectrum. Where simultaneous spectroscopy was available, both types of flare were seen to have counterparts in H α and the Ca II H line. Simultaneous time-resolved ultraviolet spectroscopy from the Goddard High Resolution Spectrograph (GHRS) aboard the *Hubble Space Telescope*, reported elsewhere, shows that at least one of the short-duration *U*-band flares was also observed in C IV with the GHRS. Time-series H α spectra showed significant evolution of the circumstellar prominence system over five consecutive stellar rotations. One prominence underwent a dramatic increase in distance from the stellar rotation axis. We speculate that this event may have been associated with one of the long-duration flares.

Key words: stars: activity – stars: individual: AB Dor – stars: low-mass, brown dwarfs – stars: magnetic fields.

1 INTRODUCTION

The chromospherically active southern K0 dwarf AB Doradus is the brightest known example of the class of ultrafast rotators observed among low-mass stars that have recently arrived on the main sequence. AB Dor has been the subject of a number of Doppler-imaging studies in recent years. The first few years of a

long-term programme of imaging studies at the Anglo-Australian Telescope (AAT) yielded observational constraints on the rate of surface differential rotation (Collier Cameron & Unruh 1994, hereafter CU94) and individual starspot lifetimes (Collier Cameron 1995, hereafter C95; Unruh, Collier Cameron & Cutispoto 1995, hereafter UCC95). More recently, (Donati & Collier Cameron 1997, hereafter DC97) have mapped the

photospheric magnetic field using Zeeman-Doppler imaging, and have shown the rate of surface differential rotation (as viewed in the corotating frame) to be almost identical to the solar value. Meanwhile, Kürster, Schmitt & Cutispoto (1994) have been conducting a similar programme at the European Southern Observatory.

The images obtained to date have shown the spot distribution on the stellar surface to be complex. The AAT observations show that during 1992 January, 1992 December, 1993 November and 1995 December the spot distribution consisted of a high-latitude polar ‘crown’ or ‘cap’ of spots encircling, and at some epochs completely covering, the visible rotation pole at latitudes of order 70° to 80° , and several discrete spots or spot groups at lower latitudes. The star is surrounded by a system of centrifugally supported prominence-like structures, which appear to be trapped in closed coronal loop structures near the Keplerian corotation radius, two or more stellar radii from the rotation axis (Collier Cameron & Robinson 1989a). The relationship between these large-scale magnetic structures and the surface spot distribution is not well understood at present. The lifetimes of individual prominence clouds appear to be on the order of a few days (Collier Cameron & Robinson 1989b). If the formation and eventual dissipation of these clouds is driven by the evolution of the distribution of magnetic flux on the stellar surface, we might reasonably expect to see a spatial correlation between the clouds and the underlying starspot distribution, and a temporal correlation between stellar flares and changes in the prominence distribution. The task of searching for such correlations is difficult, in that it requires multiwavelength time-series observations spanning several stellar rotations.

AB Dor’s rotation period of 12.4 h permits about 60 per cent of the stellar rotation cycle to be observed in a single night from any given site. The campaign described in this paper was the first in which we have used telescopes at more than one longitude in an attempt to improve the phase coverage. We achieved this by incorporating the 1994 slice of our long-term study at the AAT into the 1994 southern-hemisphere observing campaign of the Multi-Site Continuous Spectroscopy (MUSICOS) collaboration. MUSICOS is a long-standing project dedicated to the acquisition of high-resolution time-series spectra at a network of sites with full longitude coverage; results from earlier such campaigns have been described by Catala et al. (1993), Foing et al. (1994), Zhai et al. (1994), Balona et al. (1996), Böhm et al. (1996), Kennelly et al. (1996), Catala et al. (1997) and Hubert et al. (1997).

The Doppler-imaging and prominence-mapping studies of AB Doradus described here were designed to be carried out simultaneously with high-resolution UV spectroscopy from the *Hubble Space Telescope* (*HST*). Preliminary results from the *HST* observations have been published by Vilhu et al. (1998). The remainder of the present paper will therefore be devoted to the interpretation of the ground-based data on AB Dor.

In Section 2 we describe the instrumentation and the observing procedures followed at the various telescopes involved in the campaign, and present the journal of observations obtained at each site. The data reduction procedures are outlined in Section 3. The Doppler-imaging procedures are described briefly in Section 4, and the resulting surface image is discussed. Time-resolved spectroscopy of the $H\alpha$ profile shows that the slingshot prominence system surrounding the star underwent significant evolution during the campaign, and is presented in Section 5. The Ca II H & K lines were also monitored during the Doppler imaging campaign, and the results are reported in Section 6. Several flares

were observed, both in U -band photometry and in the $H\alpha$ spectra. These are described briefly in Section 5.2.

2 OBSERVATIONS

The three principal instruments used for the Doppler imaging and prominence-mapping were the Cassegrain echelle spectrograph on the 4-m telescope at CTIO, the fibre-fed MUSICOS echelle spectrograph on the 1.9-m telescope at SAAO, and the UCL coude echelle spectrograph on the 3.9-m AAT.

Of these three sites, only CTIO experienced clear weather throughout the three nights allocated to the AB Dor campaign, i.e., 1994 November 15, 16 and 17 UT. One night’s good data were obtained at SAAO on 1995 November 15, and a few hours of partially usable data were obtained at the AAT through patchy cloud on the same date.

2.1 CTIO echelle spectroscopy

The CTIO data were obtained using the long camera of the Cassegrain echelle spectrograph on the CTIO 4-m telescope. A $31.6 \text{ groove mm}^{-1}$ echelle grating was used in conjunction with a $316 \text{ groove mm}^{-1}$ cross-dispersing grating blazed at 750 nm and a GG385 blocking filter. This set-up yielded a spatial scale of 0.27 arcseconds per pixel normal to the dispersion direction, and with a $150\text{-}\mu\text{m}$ (1.0-arcsec) slit gave a resolving power $R = 31\,000$. The detector was a 2048×2048 Tektronix CCD, centred relative to the gratings in such a way as to give complete wavelength coverage over 30 orders from 563 to 774 nm. Because the chip was wider than the free spectral range, there were no gaps between orders, and indeed many spectral features located off the centre of the blaze function were recorded twice in adjacent orders. The four quadrants of the chip were read out in parallel via separate amplifiers, giving an average dead-time of 33 s between successive 150-s exposures.

The journal of CTIO observations is given in Table 1. The journal lists the sequences of individual exposures that were grouped for the Doppler-imaging study as described in Section 4 below.

2.2 AAT echelle spectroscopy

The instrumental set-up used for the AAT observations was similar to that described by C95 and UCC95. We used the UCL echelle spectrograph (Diego & Walker 1985) with a slit width of 1.2 arcsec, yielding a resolving power $R = 37\,000$. The detector, a 1024×1024 – element Tektronix CCD, was centred at 574.8 nm in order 99 of the $31.6 \text{ line mm}^{-1}$ grating, covering 43 orders from 484.7 to 744.3 nm. The free spectral range was slightly greater than the chip dimensions, leaving small gaps in wavelength coverage between the 41 orders on the chip. The chip was binned by a factor of 2 in the spatial direction to minimize readout time between exposures. An exposure time of 150 s was used for most of the AB Dor observations, in order to monitor rapid variations in the $H\alpha$ profile due to circumstellar prominence material. The dead-time of 40 s between exposures was dominated by the reading-out of the CCD in its FAST readout mode.

The journal of AAT observations is given in Table 2. The journal lists the sequences of individual exposures that were usable for time-series $H\alpha$ spectroscopy.

Table 1. Journal of CTIO observations during 1994 November 15 to 17.

| Object | UT Start 1994 Nov 15 | UT End | No of frames | Exp time [s] | Comments |
|----------|-------------------------|----------|-----------------|-----------------|---------------------------|
| HR 9087 | 00:28:31 | 00:35:41 | 3 | 120 | Standard |
| AB Dor | 00:56:34 | 03:34:52 | 35 | 150 | Group 1 |
| Gl 176.3 | 03:42:57 | 03:56:11 | 3 | 240 | K0V template |
| HR 3084 | 04:04:31 | 04:13:12 | 3 | 150 | Telluric H ₂ O |
| AB Dor | 04:33:07 | 07:16:27 | 51 | 150 | Group 2 |
| Gl 367 | 07:29:14 | 08:08:35 | 4 | 480 | M4V template |
| HR 3084 | 08:15:17 | 08:22:55 | 3 | 120 | Telluric H ₂ O |
| AB Dor | 08:30:54 | 09:11:41 | 13 | 150 | Group 3 |
| Object | UT Start 1994 Nov 16 | UT End | No of frames | Exp time [s] | Comments |
| HR 9087 | 00:34:58 | 00:39:14 | 3 | 60 | Standard |
| AB Dor | 00:51:48 | 03:36:45 | 30 | 150 | Group 1 |
| HR 3084 | 03:43:44 | 03:50:50 | 3 | 120 | Telluric H ₂ O |
| Gl 176.3 | 03:59:13 | 04:12:20 | 3 | 240 | K0V template |
| AB Dor | 04:18:30 | 07:10:48 | 54 | 150 | Group 2 |
| Gl 367 | 07:18:41 | 07:43:48 | 3 | 480 | M4V template |
| HR 3084 | 07:52:03 | 07:59:10 | 3 | 120 | Telluric H ₂ O |
| AB Dor | 08:06:29 | 09:14:00 | 27 | 150 | Group 3 |
| Object | UT Start 1994 Nov 17 | UT End | No of frames | Exp time [s] | Comments |
| HR 9087 | 00:07:06 | 00:14:15 | 3 | 120 | Standard |
| AB Dor | 00:27:50 | 03:25:48 | 35 | 150 | Group 1 |
| HR 3084 | 04:22:11 | 04:29:23 | 3 | 120 | Telluric H ₂ O |
| Gl 176.3 | 04:36:24 | 04:49:31 | 3 | 240 | K0V template |
| AB Dor | 04:56:08 | 06:55:34 | 33 | 150 | Group 2 |
| Gl 367 | 07:07:01 | 07:32:09 | 3 | 480 | M4V template |
| HR 3084 | 07:40:24 | 07:47:30 | 3 | 120 | Telluric H ₂ O |
| AB Dor | 07:54:20 | 09:06:57 | 23 | 150 | Group 3 |

Table 2. Journal of AAT observations during 1994 November 15.

| Object | UT Start 1994 Nov 15 | UT End | No of frames | Exp time [s] | Comments |
|--------|-------------------------|----------|-----------------|-----------------|----------|
| AB Dor | 09:36:26 | 09:57:55 | 7 | 150 | Group 1 |
| AB Dor | 10:42:30 | 11:45:37 | 19 | 150 | Group 2 |
| AB Dor | 13:11:29 | 13:32:56 | 7 | 150 | Group 3 |

2.3 SAAO echelle spectroscopy

The SAAO observations were secured using the fibre-fed MUSICOS echelle spectrograph (Baudrand & Böhm 1992), which was transported to South Africa from its usual location at Pic Du Midi Observatory for the duration of the 1994 MUSICOS campaign and installed on the 1.9-m telescope at SAAO's Sutherland site. The detector was a 1024×1024 Tektronix CCD. The spectrograph was used in its fixed red-wavelength configuration, covering 47 orders over the wavelength range from 514.7 to 903.9 nm, with resolving power $R = 38\,000$. Owing to the relatively small aperture of the telescope, it was necessary to use an exposure time of 240 s to obtain a satisfactory signal to noise ratio in the neighbourhood of the H α line. This was increased to 480 s during two periods of particularly bad seeing. A further overhead of approximately 66 s was incurred between successive exposures while the data were read out. As the journals of observations in Table 3 show, useful data were obtained simultaneously at both SAAO and CTIO from 1994 November 16 00:52 to 01:05 UT and 02:01 to 02:23 UT.

2.4 ESO CAT/CES spectroscopy

The profiles of the Ca II H and H ϵ lines were monitored on the nights of 1994 November 15/16 and 16/17 using the 1.4-m Coude Auxiliary Telescope (CAT) at La Silla. The detector was a thinned, back-illuminated RCA CCD of dimension 1024×640 pixels, mounted on the blue arm of the Coude Echelle Spectrograph (CES) and centred at 397.5 nm in order 57 of the echelle grating. Only a single order was recorded. This configuration yielded a resolving power $R = 40\,000$. The exposure duration was 600 s, which gave a typical signal-to-noise (S/N) ratio of 20 per pixel in the wings of the Ca II H line. Continuous coverage was obtained from 1995 November 16 03:30 to 08:57 UT, and from November 17 03:10 to 08:59 UT. The journal of CAT/CES observations is given in Table 4.

2.5 ESO optical photometry

The observations were carried out at La Silla with a single-channel photometer using an RCA31034-A0Z photomultiplier on the ESO 0.5-m automatic photometric telescope. *UBVRI* as well as narrow and wide H α filters were used. Useful data were obtained on eight consecutive nights, from 1994 November 14 to 21. In general the sky was quite good on all nights, and the observations were carried out continuously throughout, except for occasional short interruptions by moving clouds on a few of the nights. However, we found that on some of the nights the transparency varied slowly but significantly through the night.

Table 3. Journal of SAAO observations during 1994 November 15/16.

| Object | UT Start 1994 Nov 15 | UT End | No of frames | Exp time [s] | Comments |
|-------------|-------------------------|----------|-----------------|-----------------|---------------------------|
| Gl 176.3 | 20:20:43 | 20:35:43 | 1 | 900 | K0V template |
| AB Dor | 20:47:37 | 21:10:03 | 4 | 240 | Group 1 |
| AB Dor | 21:12:05 | 21:30:20 | 2 | 480 | Group 2 |
| AB Dor | 21:39:05 | 22:53:11 | 16 | 240 | Group 3 |
| HR 3084 | 22:58:50 | 23:09:03 | 2 | 240 | Telluric H ₂ O |
| AB Dor | 23:13:10 | 00:02:52 | 9 | 240 | Group 4 |
| 1994 Nov 16 | | | | | |
| AB Dor | 00:03:41 | 02:22:42 | 27 | 240 | Group 5 |
| HR 3084 | 02:29:00 | 02:41:58 | 2 | 360 | Telluric H ₂ O |
| AB Dor | 02:47:28 | 03:04:57 | 2 | 480 | Group 6 |

Table 4. Journal of CAT/CES observations during 1994 November 16 and 17.

| Object | UT Start 1994 Nov 16 | UT End | No of frames | Exp time [s] | Comments |
|-------------|-------------------------|--------|-----------------|-----------------|------------|
| AB Dor | 03:30 | 08:57 | 29 | 600 | Continuous |
| 1994 Nov 17 | | | | | |
| AB Dor | 03:10 | 08:59 | 30 | 600 | Continuous |

On the first two nights, the main purpose was to monitor flaring events on the star, and most observing time was devoted to measurements through H α and U filters, with only occasional measurements in the B , V , R and I bands. The star was observed almost continuously in the U band, with 5-s integrations. In order to maximize temporal coverage, no attempt was made to obtain differential photometry relative to comparison stars.

On the remaining six nights, the same filters were used, but the main purpose was to obtain a densely sampled $UBVRI$ light curve as an additional constraint on the surface imaging. The integration times in each filter were 50 s in the U and B bands, 25 s in V , and 30 s in R and I . Observations were also made in the narrow and wide H α filters, with integration times of 50 and 20 s respectively. Each measurement in the sequence consisted of the following set of integrations in the different filters (H α W = H α wide, H α N = H α narrow): H α W - H α N - U - B - V - R - I - I - R - V - B - U - H α N - H α W.

For these six nights, we included comparison, check and standard stars in the observing sequence. This allowed us to transform the magnitudes to the standard system, and to derive the magnitudes differentially with respect to the comparison. The

stars concerned are listed together with their positions and standard $UBVRI$ magnitudes in Table 5.

The observing programme on each night was organized in such a way that the first three standards were observed at the beginning, and the other two near or at the end of the night. The remainder of the night was devoted to a basic sequence for AB Dor, comparison and check stars. This basic observing sequence consisted of the following measurements (S - sky, C - comparison, K - check, T - target = AB Dor): S - C - T - T - T - S - K - T - T - T - S - C - T - T - T - S - C - T - T - T - ...

This basic sequence was repeated continuously, and so the comparison, HD 35474, was measured more frequently than the check, HD 36369.

3 REDUCTION PROCEDURES

3.1 Echelle spectroscopy

The spectra were extracted using the ECHOMOP echelle reduction procedures developed by Mills (1994), running on a Sun SPARCstation 10/51 system in the School of Physics and Astronomy at the University of St Andrews.

For the CTIO and AAT data, the procedures used for flat-fielding, scattered-light correction and extraction were identical to those described in CU94, and will not be repeated in detail here. To ensure compatibility between data sets obtained at different epochs and with different telescopes, spectrographs and detectors, we used the same telluric standard (BS 3084) and the same K0V and M4V spectral template stars (Gl 176.3 and Gl 367 respectively) as were used for the 1992 January data.

The four quadrants of the CTIO frames had slightly different gain factors, arising from the use of four separate amplifiers to read out the chip. To avoid small discontinuities in the spectra at the quadrant boundaries, we extracted the ‘left’ (blue) and ‘right’ (red) sides of the chip separately. We extracted the profiles of the photospheric Doppler-imaging lines Ca I 643.9 nm and Fe I 666.3 nm separately from their images in adjacent orders, where they appeared on the left and right sides of the chip respectively. The H α line and the Doppler-imaging line Ca I 671.8 nm both appeared close to the peak of the blaze function in the right half of the chip. Although these two lines were present in adjacent orders on the left half of the chip, their location in the far wings of the blaze profile yielded insufficient signal to be useful.

The wavelength calibration was performed using a third-order

Table 5. Comparison, check and standard stars used for AB Dor photometry on 1995 November 15 to 20 UT.

| Type | Name | RA2000 | DEC2000 | U mag | B mag | V mag | R mag | I mag |
|-------------|----------|------------|-----------|---------|---------|---------|---------|---------|
| Target | AB Dor | 5 28 35.7 | -65 29 17 | 8.3v | 7.9v | 7.1v | 6.6v | 6.1v |
| Comparison | HD 35474 | 5 19 51.0 | -66 05 47 | 7.92 | 7.90 | 7.51 | 7.28 | 7.05 |
| Check | HD 36369 | 5 26 32.0 | -64 21 48 | 7.54 | 7.50 | 7.48 | 7.47 | 7.45 |
| Standard 4* | E-906 | 22 40 51.6 | -44 30 14 | 9.245 | 9.193 | 8.891 | 8.713 | 8.529 |
| Standard 5* | E-911 | 22 40 51.4 | -45 12 10 | 8.566 | 8.602 | 8.124 | 7.842 | 7.560 |
| Standard 1* | E-126 | 1 33 25.5 | -43 54 7 | 9.317 | 8.660 | 7.831 | 7.375 | 6.971 |
| Standard 2* | E-303 | 6 38 47.9 | -43 49 28 | 7.469 | 7.532 | 7.562 | 7.578 | 7.594 |
| Standard 3* | E-337 | 6 32 19.4 | -45 18 34 | 9.124 | 8.249 | 7.171 | 6.611 | 6.087 |

*Data for all standard stars are taken from Menzies et al. 1989, South Africa Astron. Obs. Circ. No. 13, pp. 1–13. – $UBV(RI)_c$ Standard Stars in the E- and F-Regions and in the Magellanic Clouds – A Revised Catalogue.

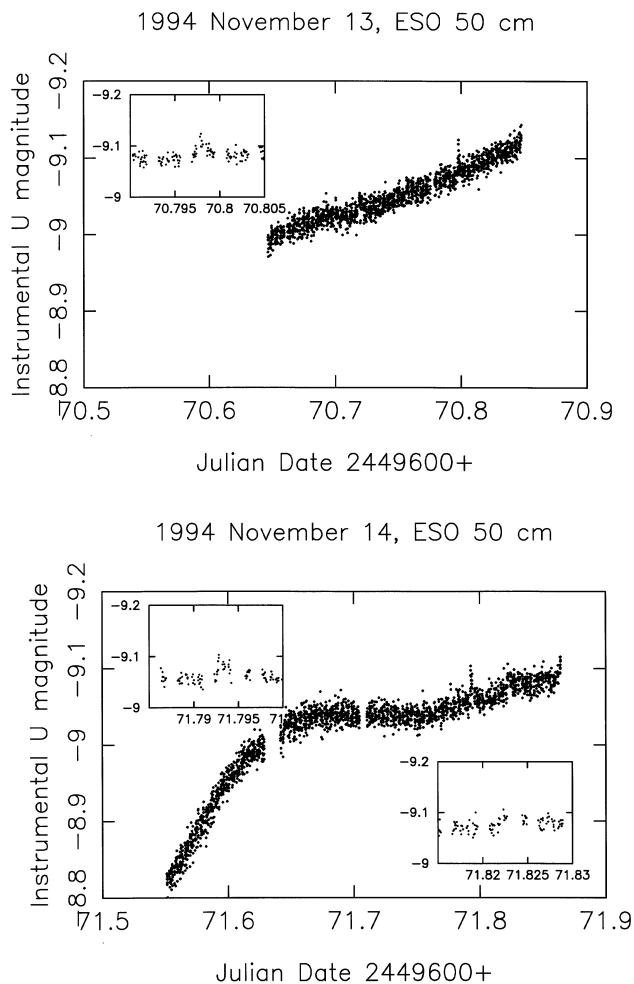


Figure 1. *U*-band photometry of AB Dor taken on the nights of (a) 1994 November 13/14, and (b) November 14/15 at the ESO 50-cm telescope. Magnitudes are given in the instrumental system and are uncorrected for extinction. Portions of the light curves around the three flares are shown enlarged.

(quadratic) polynomial fit to a thorium-argon comparison spectrum. Between 10 and 20 arc lines were used per order, yielding fits with a typical rms scatter of 3×10^{-4} nm.

The CAT/CES spectra of Ca II H and He were also extracted with ECHOMOP, and were calibrated in wavelength in the same way as the H α spectra.

3.2 *UBVRI* photometry

The dead time for the photomultiplier RCA31034-A0Z was 7.5×10^{-9} s. Even for the highest count-rate, $34000 \text{ count s}^{-1}$, the correction is less than one part in one thousand. In practice, there was therefore no need to apply a dead-time correction.

The *U*-band observations on the first two nights were reduced to sky-subtracted instrumental magnitudes, with no attempt made to correct for extinction or to transform the data to the standard system. The resulting light curves (Fig. 1) show the effects of slow changes in transparency during the night. This does not affect the main purpose of these observations, which was to search for short-duration optical flare events.

One flare event was observed on the first night, at HJD 244 9670.798, with a peak amplitude $\Delta U = 0.04$ mag. The rise

time was between 10 and 30 s, and the decay time between 60 and 100 s. The *U*-band light curve published by Rucinski (1995), which was obtained at Las Campanas simultaneously with our observations, shows only a single high-flux measurement during the decay phase of this flare, which evidently occurred while Rucinski was making a comparison-star measurement! We conclude that this event was almost certainly a genuine flare, because it coincided precisely with the third of three short-duration flares in the C IV doublet at 1548.202 and 1550.774 Å, observed with the *Hubble Space Telescope* by Vilhu et al. (1998). Unfortunately, this flare occurred right at the end of the GHRS observation, and the decay phase in C IV was not observed. Curiously, two flares with even greater amplitudes were observed in C IV at HJD 244 9670.6837 and 244 9670.7179. These have no clearly identifiable *U*-band counterparts in either Rucinski's data or ours. Conversely, we do not see any evidence of a flare at HJD 244 9670.82, when Rucinski's data show another isolated high point.

The two flares seen on the second night were, however, observed independently by ourselves and by Rucinski. The first, at HJD 244 9671.793 (rotation phase 10441.574), had a peak amplitude of 0.04 mag, a rise time between 10 and 30 s, and a decay time of order 100 s, with a possible secondary peak 104 s after the initial rise. The second, at HJD 244 9671.823 (phase 10441.632), had an amplitude of at most 0.02 mag in our data. While the main panel shows evidence of a small disturbance, the expanded plot at the lower right shows only a rather leisurely increase just prior to this time, followed by a gap in the data for a sky background observation beginning at HJD 244 9671.8225. Rucinski's light curve shows the amplitude of this flare to be closer to 0.03 mag, with the peak at HJD 244 9671.823, which suggests that we may have missed the peak during the sky measurement. The decay time appears to have been slightly longer for this flare than for the others, perhaps on the order of 100 to 200 s. Significantly, Rucinski's observations were made using a CCD as the detector, and Rucinski reported that the dMe-star companion, Rst 137B, was not seen in any of the images. This confirms that these flares originated on AB Dor itself, and not on Rst 137B.

As mentioned in Section 2.5, on the last six nights we included comparison, check and standard stars in the observing sequence. This allowed us to transform the magnitudes to the standard system and to derive the magnitudes differentially with respect to the comparison. This was done on one of the workstations at La Silla, using the ESO program RANBO2.

The differential magnitudes were derived by linear interpolation of the comparison-star magnitude as a function of time. The *V*- and *U*-band light curves shown in Fig. 2 were computed in this way, then translated back into standard magnitudes assuming that $V = 7.51$ and $U = 7.92$ for the comparison star HD 35474. The 18 observations of the check star HD 36369 yielded $V = 7.473$ and $U = 7.548$, again assuming $V = 7.51$ and $U = 7.92$ for the comparison. The rms scatter in the differential magnitudes for the check star was 0.006 mag in *V* and 0.005 mag in *U*.

There is clear evidence of stochastic night-to-night variability in the light curves, particularly in the *U* band. As is discussed below, not all of the night-to-night changes can be attributed to the effects of differential rotation. In particular, a long-duration *U*-band flare, with a maximum amplitude of 0.1 mag, peaked at HJD 244 9674.594, just after rotation phase 10447.0. At the peak of this flare, the *V* magnitude of the star was 0.03 mag brighter than was observed on the preceding and following days at the same

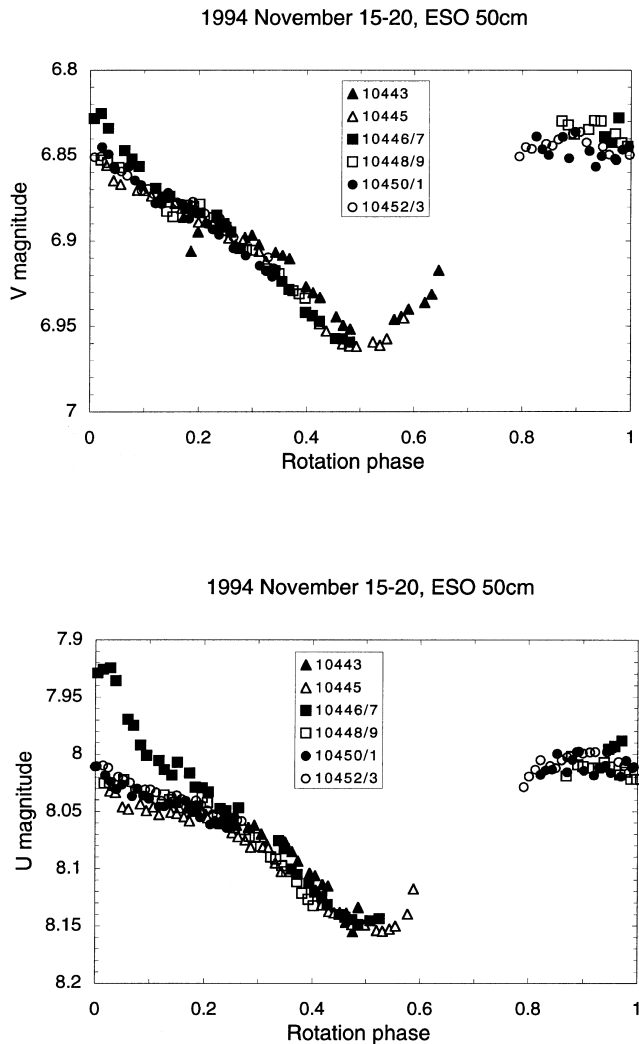


Figure 2. The light curve of AB Dor in the V and U bands, obtained with the ESO 50-cm telescope on 1995 November 15–20. The data were folded using the ephemeris $\text{HJD} = 244\,4296.575 + 0.51479E$. The legend shows the association between the symbol used to plot each day’s observations and the rotation number.

rotation phase. The rise time for this flare appears to have been less than 20 min. Following the flare peak, the U -band enhancement decayed on an e-folding time of just under 2 h. Regrettably, there were no simultaneous spectroscopic observations of this flare.

A second optical continuum flare event of similar duration may account for the apparent discrepancy between the U and V light curves between rotation phases 0.3 and 0.5 on the first two nights of this run. The discrepant light curve is that for 1994 November 15/16 (rotation 10443), marked by filled triangles. This event peaked at $\text{HJD} 244\,9672.73$ (rotation 10443.4), and had a total duration of 0.2 rotation cycles – just under 3 h – in both bands. More curiously, the flare enhancement was no greater in the U band than in V , having an amplitude of order 0.02 mag in both bands. This long-duration flare was also observed in $H\alpha$ and the Ca II H line, as is discussed later in the paper.

4 DOPPLER IMAGING

Because of the lower signal to noise ratios of the SAAO and AAT

data, and the lack of continuum and telluric-line standards for the AAT data, only the CTIO data were used for Doppler imaging. The image reconstructions were carried out on least-squares deconvolved (LSD) profiles derived from the large number of intermediate-strength photospheric lines recorded in each echellogram. The deconvolution method is described in detail by Donati et al. (1997).

The surface images were reconstructed using DOTS, a maximum-entropy code for performing Doppler tomography of stellar surfaces. The stellar surface geometry model and integration scheme of the version used here are designed for dealing with high signal to noise profiles, and are described by Collier Cameron (1997). The look-up tables of specific intensity profiles required by DOTS were generated from the observed profiles of same lines in the spectral template stars G1 176.3 (K0V, representing the photosphere), and G1 367 (M4V, representing the spots). This was achieved by using the same deconvolution procedure on the template stars as was used for the spectra of AB Dor. The minimum of the deconvolved profile of each of the two template stars was then shifted to zero radial velocity. Finally, the look-up tables were produced by scaling the continua of the observed spectra as described by Unruh & Collier Cameron (1995). We used separate linear limb-darkening laws for the photosphere and spots, computed from interpolated ATLAS9 model atmospheres (Kurucz 1993) with effective temperatures of 5000 and 3500 K respectively, at the weighted mean line wavelength of 640 nm.

4.1 Data preparation

Each echellogram covered the wavelength range from 549.55 to 793.23 nm, with significant overlap between adjacent orders. The deconvolution utilized profile information from all photospheric absorption lines in this range with central depths between 0.4 and 0.95 times continuum, as calculated from ATLAS9 model atmospheres and line lists (Kurucz 1993) for a star of spectral type K1, and kindly provided by Dr J.-F. Donati (personal communication). Four wavelength ranges, from 627.5 to 632.0 nm, 686.6 to 704.1 nm, 716.7 to 733.6 nm, and 759.2 to 770.4 nm, were excluded because of pollution by strong telluric absorption bands. In all, the deconvolution was based on a total of 1361 images of 674 photospheric absorption lines.

The deconvolution process is particularly sensitive to systematic errors in continuum fitting, since the continuum must be subtracted prior to cross-correlation with the weighted line list. To ensure maximum consistency between the continuum fits to the photospheric template spectrum and to the spectra of AB Dor, we first computed an iterative floating 11th-order polynomial fit to the continuum of the template spectrum. The template spectrum was divided by this fit and artificially broadened and shifted, to approximate the rotational broadening and radial velocity of AB Dor. Next, we co-added a group of AB Dor spectra, to serve as a master reference spectrum. This reference spectrum was divided through by the broadened, shifted template, and a new polynomial continuum fit was derived.

The reference spectrum and its continuum fit were used to ensure that subsequent fits to all the AB Dor spectra were homogeneous. Close examination of the raw data revealed slowly varying changes in the low-frequency structure of the stellar continuum, which could possibly have been caused by small misalignments in the spectrograph optics. Whatever the cause, the effect was removed successfully by dividing each individual

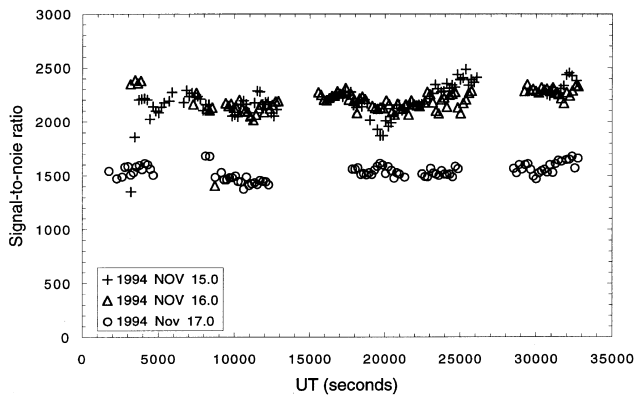


Figure 3. The S/N ratio of the deconvolved photospheric line profiles derived from the CTIO echelle spectra, plotted as a function of time in seconds from UT 1994 November 15.0, 16.0 and 17.0. Symbols denoting different dates are given in legend.

echellogram of AB Dor by the reference spectrum and median-smoothing the result with a box size of 100 pixels. This yielded a map of correction factors that were applied to the master continuum frame during processing of the individual echellograms.

The deconvolved profiles comprised 70 pixels in the dispersion direction, with a uniform velocity increment of 3.5 km s^{-1} per pixel. The signal to noise ratios per pixel of the deconvolved profiles were computed from the diagonal elements of the deconvolution matrix, using Poissonian errors propagated through the data extraction process. As a secondary check, we also assessed the errors empirically from the scatter in the pixel values in the continuum immediately adjacent to the absorption wings of the deconvolved profiles. We found that in general the empirical errors were 20 to 50 per cent greater than those computed from photon noise alone, on any given night. We scaled the computed errors accordingly, to ensure that the MaxEnt reconstruction process would yield a satisfactory fit to the data at $\chi^2 \approx 1$. The continuum signal to noise ratios of the resulting deconvolved profiles are plotted as a function of time in Fig. 3. The mean signal to noise ratios were found to be of order 2200 on the first two nights, and 1500 on the third. The depth of the deconvolved profile was 3.5 per cent below the continuum level, so that the ratio of the profile depth to the rms noise amplitude was approximately 70 on the first two nights, and 50 on the third.

The resulting dynamic spectra are plotted in grey-scale form in Figs 4 to 6, together with the model spectra and residuals computed from the reconstructed images. To enhance contrast, profiles computed from a featureless model star have been subtracted from the dynamic spectra. The resulting difference spectra show many bright signatures of low-latitude spots crossing the stellar disc, with excellent night-to-night repeatability. The enhancement of the line core and the corresponding depression of the line wings relative to the ‘immaculate’ profile constitute the evidence for the extensive spot activity seen at high latitudes in the reconstructed images.

4.2 Reconstruction procedure

The image reconstruction was performed using the MEMSYS algorithm described by Skilling & Bryan (1984).

For the case where the reconstruction is based on spectroscopic data alone, this amounts to finding an extremum of the function

$Q(f) = S(f) - \lambda\chi^2(f)$, where f is a vector whose elements correspond to the individual pixel values in the image, and $\chi^2(f)$ quantifies the degree of misfit between the observed spectra and their synthetic counterparts, computed from the image f .

Starting from a blank initial image, the code was allowed to refine the image iteratively by adjusting the value of λ until the absolute value of the image entropy (or equivalently, the fraction of the stellar surface occupied by spots) began to increase rapidly as χ^2 was driven lower. As C95 describes, this marks the point at which the image begins to develop spurious fine structure through attempting to over-fit noise features in the data, and the reconstruction process was stopped at this point.

4.3 Fine-tuning of stellar parameters

The stellar radial velocity, $v \sin i$ and line equivalent width are important free parameters, whose values must be determined before a surface image can be recovered reliably from the data. We determined these parameters initially using the spot-area minimization method described by CU95.

The values were then refined further by driving the value of χ^2 as low as possible, and adjusting the parameters to eliminate systematic misfits in the far wings of the profile. We achieved this by subtracting the model fit from the actual data, and co-adding all the resulting residual profiles for each night separately. At the very high signal to noise ratios thus achieved, the far wings of the residual profile are predominantly sensitive to errors in $v \sin i$ and radial velocity. We found that the values of 90 to 91 km s^{-1} that we have used in previous imaging studies of AB Dor gave a systematic misfit in the far wings, of the type that is expected to result from over-estimation of $v \sin i$. Altering the EW of the line did not eliminate the misfit. We found instead that $v \sin i = 89.5 \text{ km s}^{-1}$ gave the best fit to the line wings on all three nights. This is somewhat less than the 90 to 91 km s^{-1} that we have adopted in earlier work, but the higher signal to noise ratio of the present observations suggests that the lower value is more appropriate. The best-fitting radial velocities were 31.5, 29.5 and 31.5 km s^{-1} for the three nights of the CTIO run, the scatter being due mainly to small systematic errors in the nightly wavelength calibrations.

4.4 The reconstructed images

In CU94, we introduced a weighting scheme for the assessment of the goodness-of-fit statistic χ^2 , which was designed to suppress the contribution of those parts of the data (i.e., the surrounding continuum) which were insensitive to changes in the spot distribution on the visible stellar hemisphere. Subsequent experimentation showed that this scheme had the undesirable effect of suppressing the contribution of distortions in the line wings, caused by low-latitude spots near the stellar limb. In the new version of the DOTS code, all points within $\pm v \sin i$ of the line centre are accorded uniform weights in the calculation of χ^2 , while those outside the part of the profile affected by spots are given zero weight. This prevents dilution of the χ^2 statistic by invariant parts of the data, while allowing features in the line wings to contribute as they should. We thus expect the new version to give a more faithful reconstruction of any low-latitude features present.

The effective number N_{eff} of data points that contribute to χ^2 under this weighting scheme gives us some idea of the value to

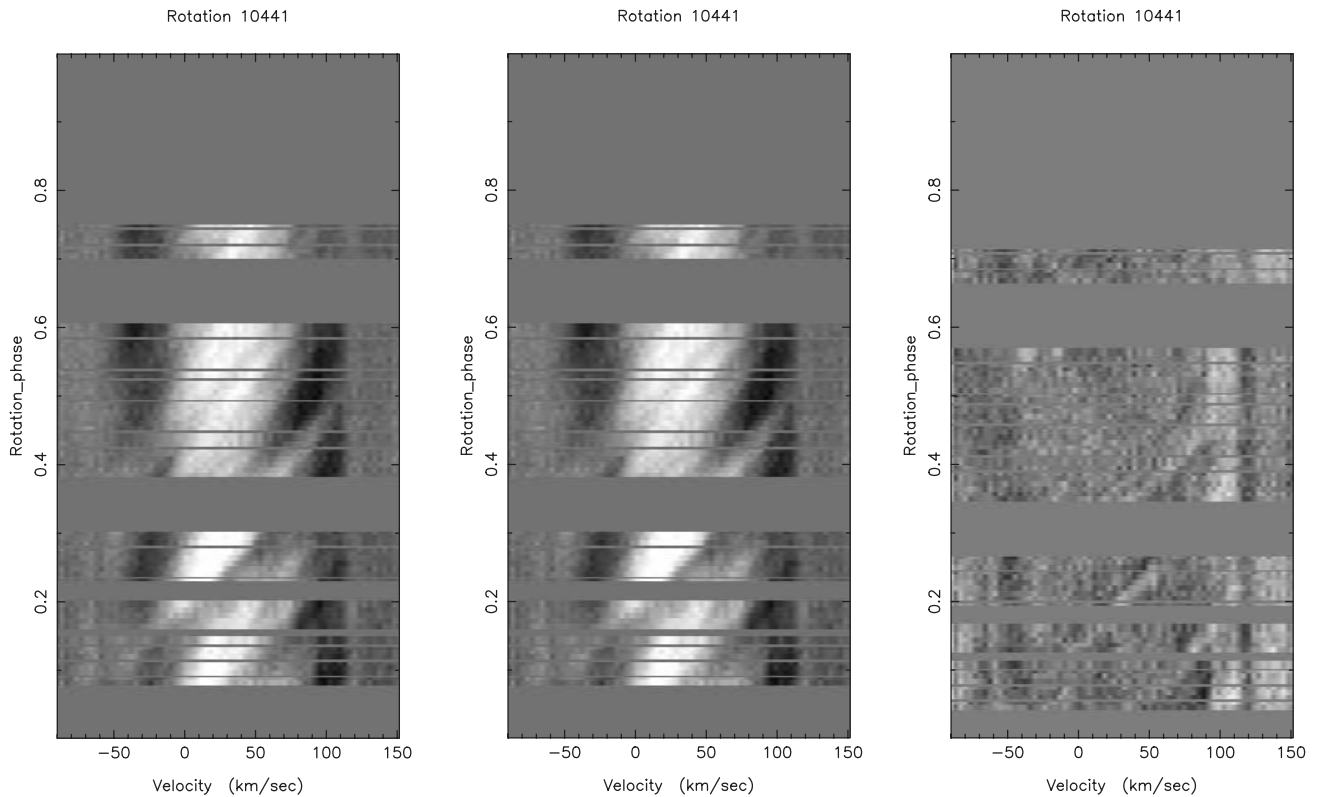


Figure 4. Dynamic spectrum of least-squares deconvolved photospheric line profile distortions for the night of 1994 November 14/15. Panels (a) and (b) show the data and the model dynamic spectrum derived from the reconstructed images. A model profile derived from an unspotted surface map has been subtracted to enhance the contrast of the starspot signatures. The grey-scale is linear, with black at -0.005 times the continuum signal level and white at $+0.005$ times continuum. Panel (c) shows a map of the residuals after subtracting the model from the data. The residuals are divided by the error estimates, and the grey-scale runs from black at -5σ to white at $+5\sigma$. The heliocentric velocity scale is in km s^{-1} , and the rotation phases up the left side of each diagram are computed according to the ephemeris of Innis et al. (1988).

which χ^2 should converge without over- or under-fitting the data. At first, we sought to fit the spectroscopic data independently of the photometry. The goodness-of-fit parameter χ^2/N_{eff} of the resulting image had a value of 1.3 at the optimum stopping point in all three cases. This indicates a satisfactory fit to the data, given that the error bars were indeed representative of the rms scatter of the data. The resulting images for the three nights of the run are shown in Figs 7 to 9. The right-hand panels of Figs 4 to 6 show no systematic residuals with amplitudes greater than about twice the rms noise amplitude in the fits to the spectra.

As with previous instances (UGC95) in which we have used spectroscopy and photometry as simultaneous constraints on the image, we found that images derived using spectroscopy alone tended to suppress slightly the strengths of low-latitude features, giving a light curve whose minimum occurred at the correct phase but whose amplitude was lower than observed (Fig. 10). To overcome this problem, we introduced the broad-band photometry obtained at ESO in the *V*, *R* and *I* bands during the third night of the CTIO run, as additional constraints on the reconstructed image for that night. This was not possible for the first two nights, owing to the absence of *VRI* photometry on November 14 and the optical flare on November 15.

When two different types of data are used, the image reconstruction problem involves maximizing the value of an entropy function S along the intersection of two independently defined constraint surfaces for the spectroscopic and photometric

data sets (Collier Cameron, Jeffery & Unruh 1992). This entails finding the extremum of the function $Q(f) = S(f) - \mu\chi_s^2(f) - \nu\chi_p^2(f)$. The degrees of misfit between the observed spectra and light curves and their synthetic counterparts are quantified by χ_s^2 and χ_p^2 respectively. The coefficients μ and ν are Lagrange multipliers whose values are to be determined. The two χ^2 statistics can be combined with an appropriate weighting factor β to give $\chi_t^2 = \beta\chi_s^2 + (1 - \beta)\chi_p^2$. The problem then reduces to finding an extremum of $Q(f) = S(f) - \lambda\chi_t^2(f)$, where $\mu = \lambda\beta$ and $\nu = \lambda(1 - \beta)$. In order to achieve a satisfactory fit to both the spectroscopic data and photometric data simultaneously, it is necessary to adjust the weighting parameter β by trial-and-error until a satisfactory fit is obtained to both data sets simultaneously. Too low a value of β overfits the photometry at the expense of the spectroscopy, and vice versa.

A weighting factor $\beta = 0.50$ was found to give a moderately satisfactory fit to both types of data simultaneously, at a value of $\chi_s^2/N_{\text{eff}} = 1.28$, and $\chi_p^2/N_{\text{phot}} = 1.30$, similar to the value achieved when the spectra were used as the sole constraints on the image.

Inclusion of the photometric data as an additional constraint had no perceptible effect on the fits to the dynamic spectra. The amplitudes of the photometric light curves can be seen still to be slightly underestimated in the *V* band (Fig. 10) and slightly overestimated in the *I* band. At face value, this suggests that the spot temperature may have been set too low, giving too great a contrast between spot and photosphere in the *I* band. We note,

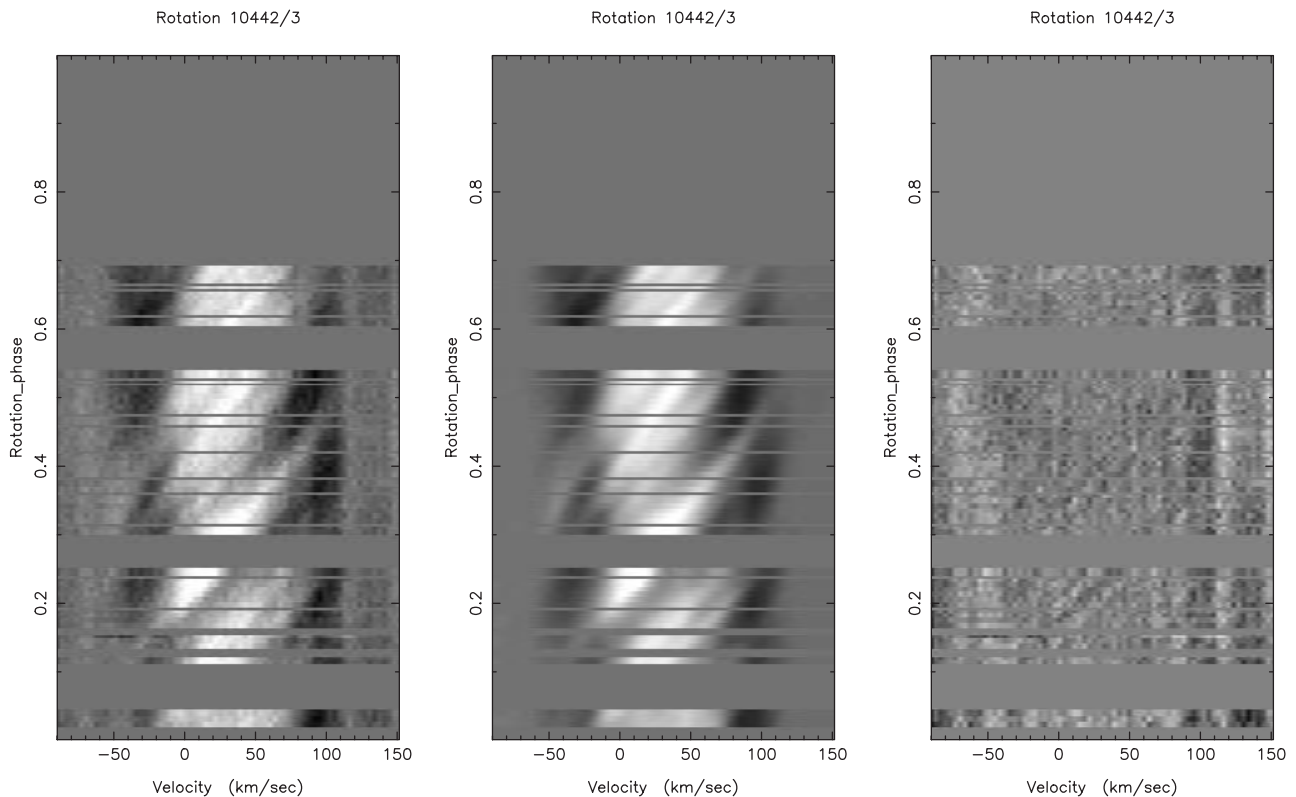


Figure 5. As for Fig. 4, for the night of 1994 November 15/16.

however, that the Kurucz models on which the photometric intensities are based do not take account of the presence of TiO bands at red wavelengths in the spectrum of the spots. A slight misfit to the relative amplitudes at the different wavelengths is not therefore too surprising.

This misfit does, however, have the undesirable effect that it makes the reconstruction algorithm tend to over-fit any noise that is present in the photometry. This leads to some fragmentation of the reconstructed image (Fig. 11). Aside from this, the principal effect of including the photometry as an additional constraint is to improve the latitude discrimination in the equatorial region. This is apparent from a comparison of Fig. 9, which was derived from spectra only, with Fig. 11. In particular, the two spot groups at longitudes 300° to 330° and longitude zero are forced to appear at the same (absolute) latitudes as before, but in the hemisphere that is turned away from the observer. This is confirmed by direct inspection of Figs 4 to 6. The bright double feature representing the spots between longitudes 300° and 330° cross the centre of the profile at phases 0.1 to 0.17, and clearly do not extend into the wings of the profile. The higher latitude spot at longitude 260° produces a trail that crosses the centre of the profile at phase 0.27, and which clearly extends into the profile wings.

This ability of photometry to resolve ‘mirror-image’ hemispheric ambiguities of this kind is very useful. We note, however, that even if a feature is reconstructed in the wrong hemisphere, its latitude (in the absolute sense) is likely to be reproduced reasonably reliably even in the absence of photometry. This means that differential rotation studies such as those of DC97 and Donati et al. (1999) do not require simultaneous photometric support – provided, of course, that the differential rotation pattern is symmetric about the equator!

5 $H\alpha$ PROMINENCE MAPPING

The $H\alpha$ profile of AB Doradus is characterized by strong, transient absorption features, which cross the rotation profile of the star over an interval of an hour or so. Previous studies have shown that the pattern of absorption transients repeats itself at intervals of one stellar rotation, but that significant changes can occur on time-scales of order 24 h.

The observations obtained during the MUSICOS 94 campaign span five consecutive stellar rotations. Poor weather at the AAT and SAAO precluded full phase coverage over this period.

The lack of telluric and continuum standards for the AAT data prevented us from employing our usual continuum fitting and telluric-line corrections for the few data collected at the AAT. We opted to settle for a third-order polynomial fit to several local continuum windows near $H\alpha$, and we did not attempt to remove the telluric features from these data.

The $H\alpha$ spectra from all sites were rebinned to a linear velocity scale with 2.5 km s^{-1} per bin, which is close to the pixel scale of the raw data in all cases. The signal to noise ratio per pixel in the rebinned spectra was approximately 270 in the continuum near $H\alpha$ on all three nights for the 150-s exposures from CTIO. The signal to noise ratio of the AAT data was variable owing to the patchy cloud cover, but ranged between 30 and 50 in the usable parts of the data set. The signal to noise ratio of the SAAO data was between 50 and 60. Finally, the spectra were normalized to unit flux in the fitted pseudo-continuum and phase-binned, treating each consecutive rotation separately. The full time resolution of the data was preserved in order to permit tracking of any rapidly moving

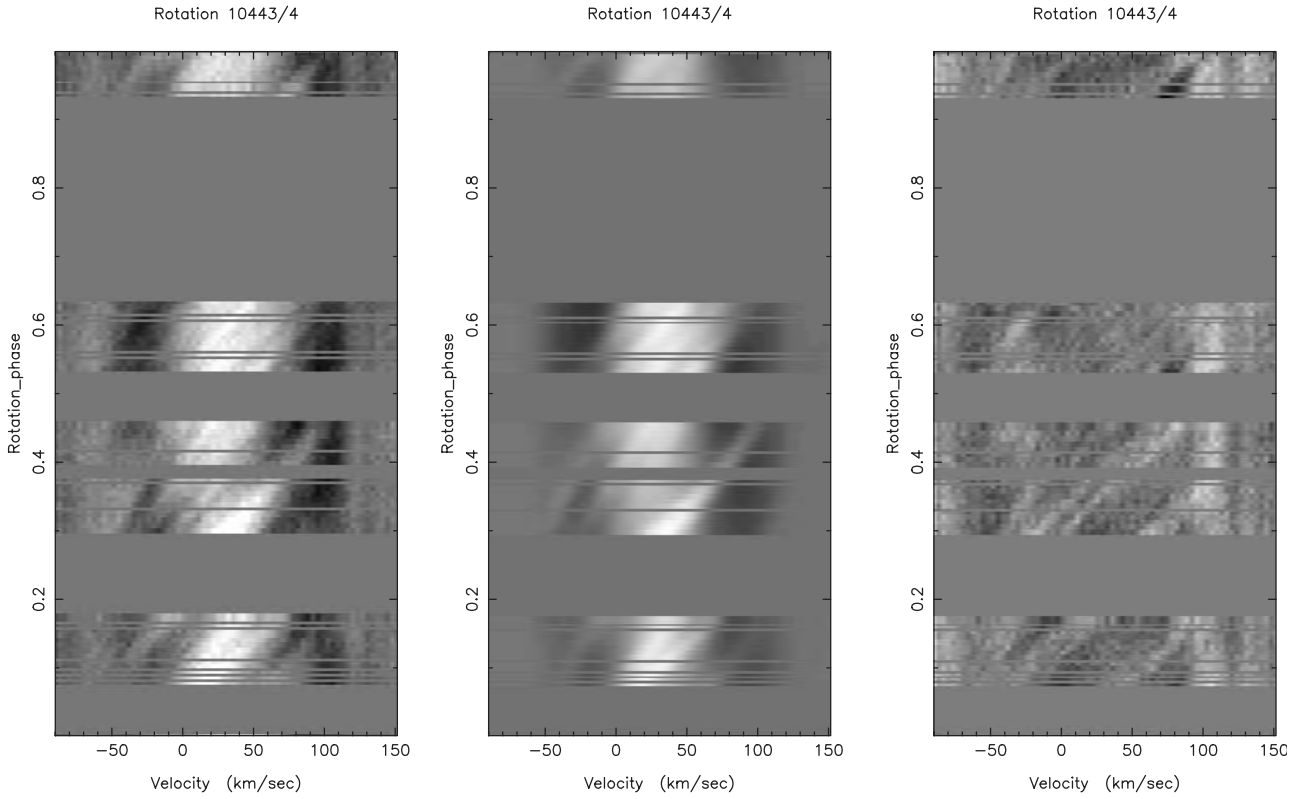


Figure 6. As for Figs 4 and 5, for the night of 1994 November 16/17.

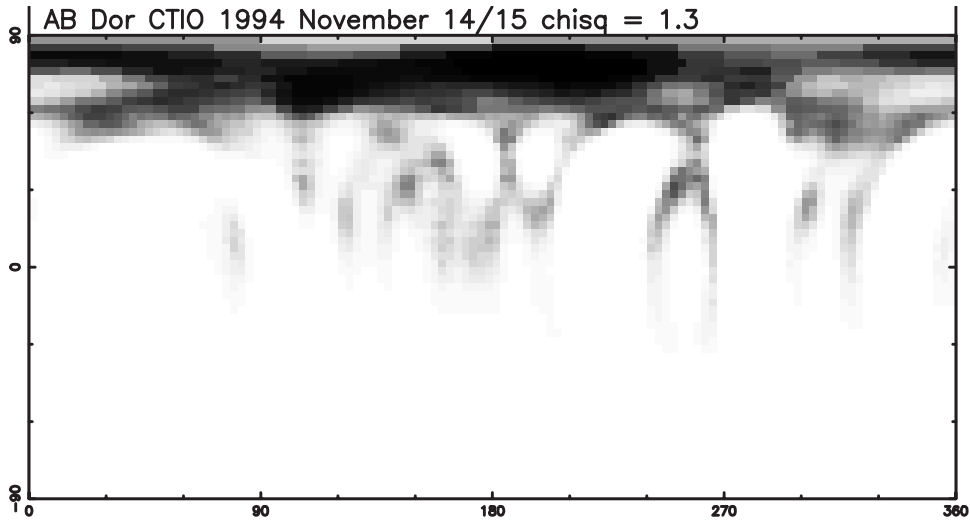


Figure 7. The starspot distribution on AB Dor on 1994 November 14/15 UT, derived from the least-squares deconvolved rotation profiles from CTIO spectra as shown above. The synthetic data derived from this image give a reduced $\chi^2 = 1.3$. The grey-scale runs from black at 100 per cent spot occupancy to white at zero spot occupancy per pixel.

features. The resulting dynamic spectra are illustrated in grey-scale form in Fig. 12.

5.1 Absorption transients

While the signal to noise ratios of the AAT and SAAO data are lower than those of the CTIO data, they are none the less sufficient to allow the pattern of transients to be followed in detail. A list of the major transients is given in Table 6. Where the data allow, their

drift rates $\dot{\varpi}$ have been measured and converted to axial distances ϖ in units of the stellar radius R_* using

$$\frac{\varpi}{R_*} = \frac{\dot{\varpi}}{\Omega v \sin i},$$

where Ω is the stellar angular velocity in radians per second, $\dot{\varpi}$ is measured in km s^{-2} , and $v \sin i$ is measured in km s^{-1} . The drift rate was measured in each case by taking the first derivative of Fig. 12 in the time direction. This procedure gives a sharp

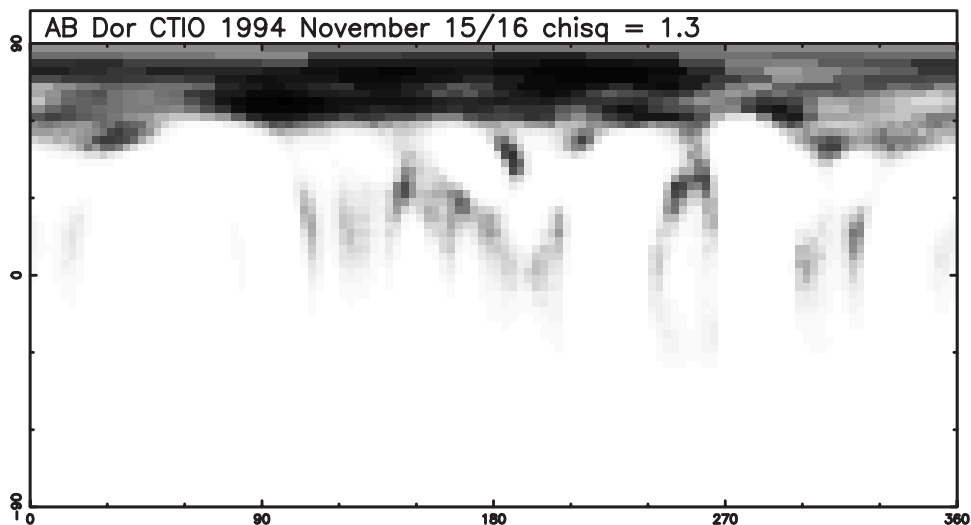


Figure 8. The starspot distribution on AB Dor on 1994 November 15/16 UT, derived from CTIO spectra. The synthetic data derived from this image give a reduced $\chi^2 = 1.3$. The grey-scale is the same as in Fig. 7.

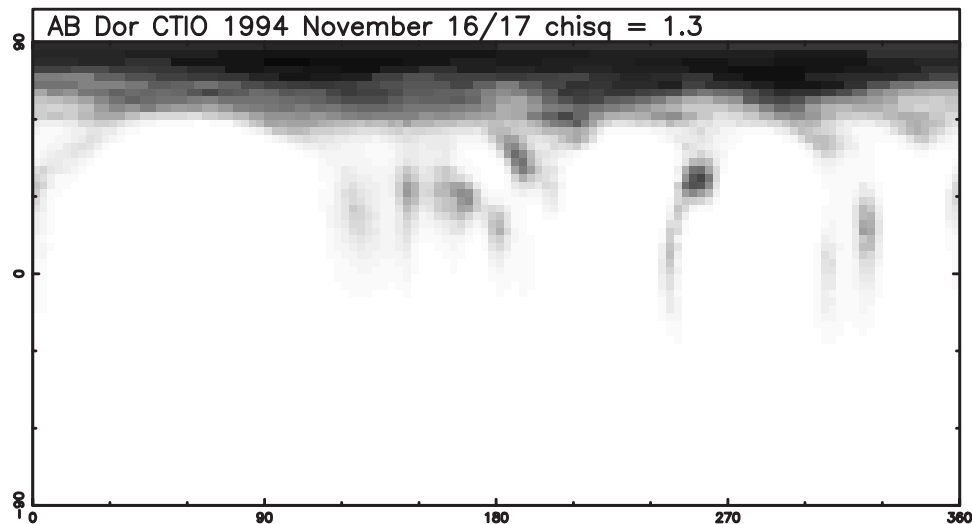


Figure 9. The starspot distribution on AB Dor on 1994 November 16/17 UT, derived from CTIO spectra. The synthetic data derived from this image gives a reduced $\chi^2 = 1.3$. The grey-scale is the same as in Fig. 7.

transition from positive to negative values along the main ‘ridge line’ of each transient. The location of this transition was determined for each transient in each individual time slice of the map. A linear fit to the resulting time-series of ridge-line wavelengths yielded the drift rate together with 95 per cent confidence limits and the phase of meridian crossing for each transient observed.

Several features are worth noting.

(i) A large number of transient absorption features were observed, more or less uniformly distributed in rotation phase.

(ii) The strongest transient was centred at rotation phase 0.00. It was observed in its entirety from both CTIO and SAAO during rotation 10442/3, and partially from CTIO at the end of rotation 10444. It was missed on the other three rotations due to incomplete phase coverage.

(iii) There is no clear relationship between the longitudes of the slingshot prominences giving rise to the transients, and the underlying starspot distribution.

(iv) Although many of the prominence features are seen to reappear on successive rotations, the detailed structure of the prominence system evolved significantly over the five rotations observed. Unfortunately, the timing of the transients with respect to gaps in the data precludes reliable measurement of their individual rotation periods. Inspection of Fig. 12 suggests that transients D and G may lag slightly behind the overall stellar rotation, but without precise meridian-crossing timings throughout the run it is difficult to draw any firm conclusions. Transient G, first seen at phase 10441.557, persists throughout the run, but is partially obscured on rotation 10445 by a very rapidly moving transient, F

(v) Transient F has no obvious counterpart at the same phase in

any of the earlier exposures. The radial acceleration of transient F places it reliably at 8 stellar radii from the rotation axis. This very rapid radial acceleration of individual clouds has been documented on two other occasions in AB Dor, on 1986 November 15 (Collier Cameron & Robinson 1989b) and on 1996 December 25 (Donati et al. 1999). On the latter occasion, the rapid transient was seen to have disappeared after four further rotations. We consider it likely that the precursor of F may have been transient E, which on rotations 10441 and 10443 appeared at phases 0.46 and 0.48, becoming more sharply defined but lagging perceptibly behind the rotation of the star and the rest of the prominence system. This type of behaviour has been observed previously by Collier Cameron & Robinson (1989b), who interpreted it as being due to an increase in the distance of the absorbing cloud from the star. The lag in phase can then be interpreted as an attempt by the cloud

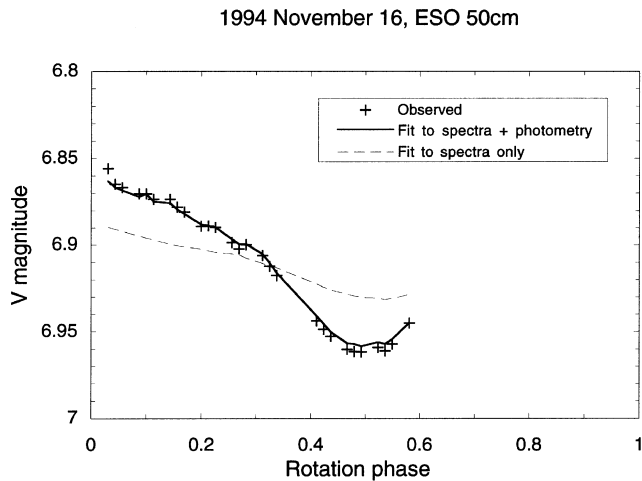


Figure 10. The V-band light curve of AB Dor on 1994 November 16/17 UT, from the ESO 50-cm telescope. The dashed line shows the light curve predicted from an image reconstructed from spectral data alone, while the solid line shows the fit from an image recovered using both spectra and *VRI* photometry as constraints. The latter fit gives a reduced $\chi^2 = 1.3$ for both spectral and photometric data.

to conserve angular momentum as its confining structure expands outward, possibly heralding centrifugal ejection of the cloud material.

(vi) Significant amounts of absorption are present on several occasions at wavelengths significantly greater than 656.55 nm, which corresponds to the velocity of the receding limb of the star. These redshifted absorptions are seen at times when a strong prominence complex is moving off the receding limb of the star, notably at rotation phases 10441.50, 10443.403, 10445.40 and 10445.57. The last of these appears to be associated with the rapidly moving transient described above.

5.2 Flare activity in H α

A short-lived enhancement of the H α emission occurred during exposure 236, which started at 1994 November 15 07:01:44 UT and ended at 07:04:14 (rotation phase 10441.574). Note that this coincides with the first of the two *U*-band flares observed at ESO and Las Campanas on this night, with the rise and decay having occurred almost entirely within the 150-s duration of the H α exposure. As a result of its short duration, this flare is only just visible in Fig. 12(a). It appears as a thin, bright horizontal streak displaced slightly to redward of line centre at phase 0.574. The profile was isolated by subtracting the mean profile seen in exposures 235 and 237 from that obtained in 236 (Fig. 13). The resulting flare profile was symmetric and triangular. A least-squares Lorentzian fit to the residual profile yielded a peak height 0.027 times continuum, half-width at half-maximum intensity $63.4 \pm 2.0 \text{ km s}^{-1}$ and centroid radial velocity $63.5 \pm 2.0 \text{ km s}^{-1}$.

A more long-lived enhancement of the H α emission was seen between phases 0.34 and 0.45 during rotation 10443, i.e., from HJD 244 9672.701 to 244 9672.762. The enhancement was not seen when the same range of phases was observed during rotations 10441 and 10445, and appears to represent a flare of much longer duration than the rapid event seen at phase 10441.574.

6 Ca II H AND H ϵ PROFILE VARIABILITY

The blue spectra from the CAT/CES were processed in the same way as the H α time-series data from the larger telescopes, and

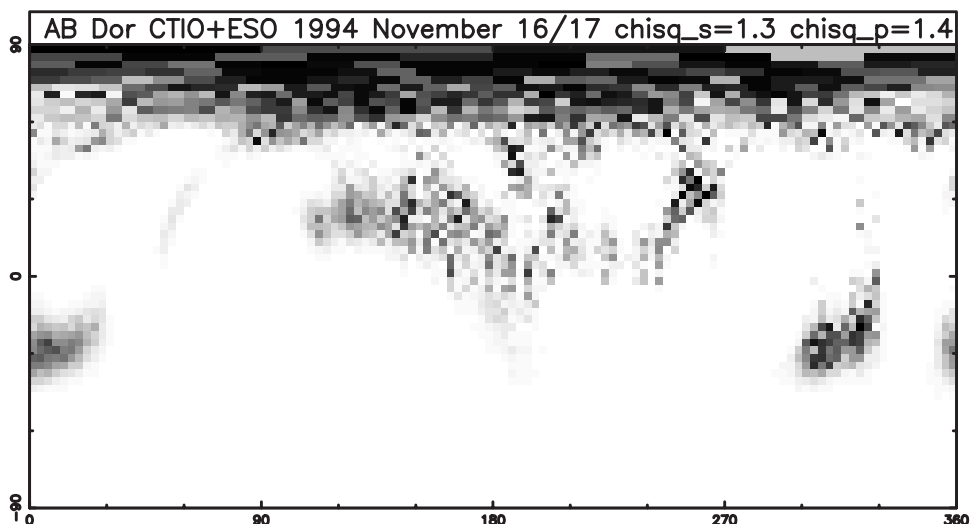


Figure 11. The starspot distribution on AB Dor on 1994 November 16/17 UT, derived from CTIO spectra and ESO *VRI* photometry. The synthetic data derived from this image gives a reduced $\chi^2 = 1.3$ for both spectral and photometric data. The grey-scale is the same as in Fig. 9.

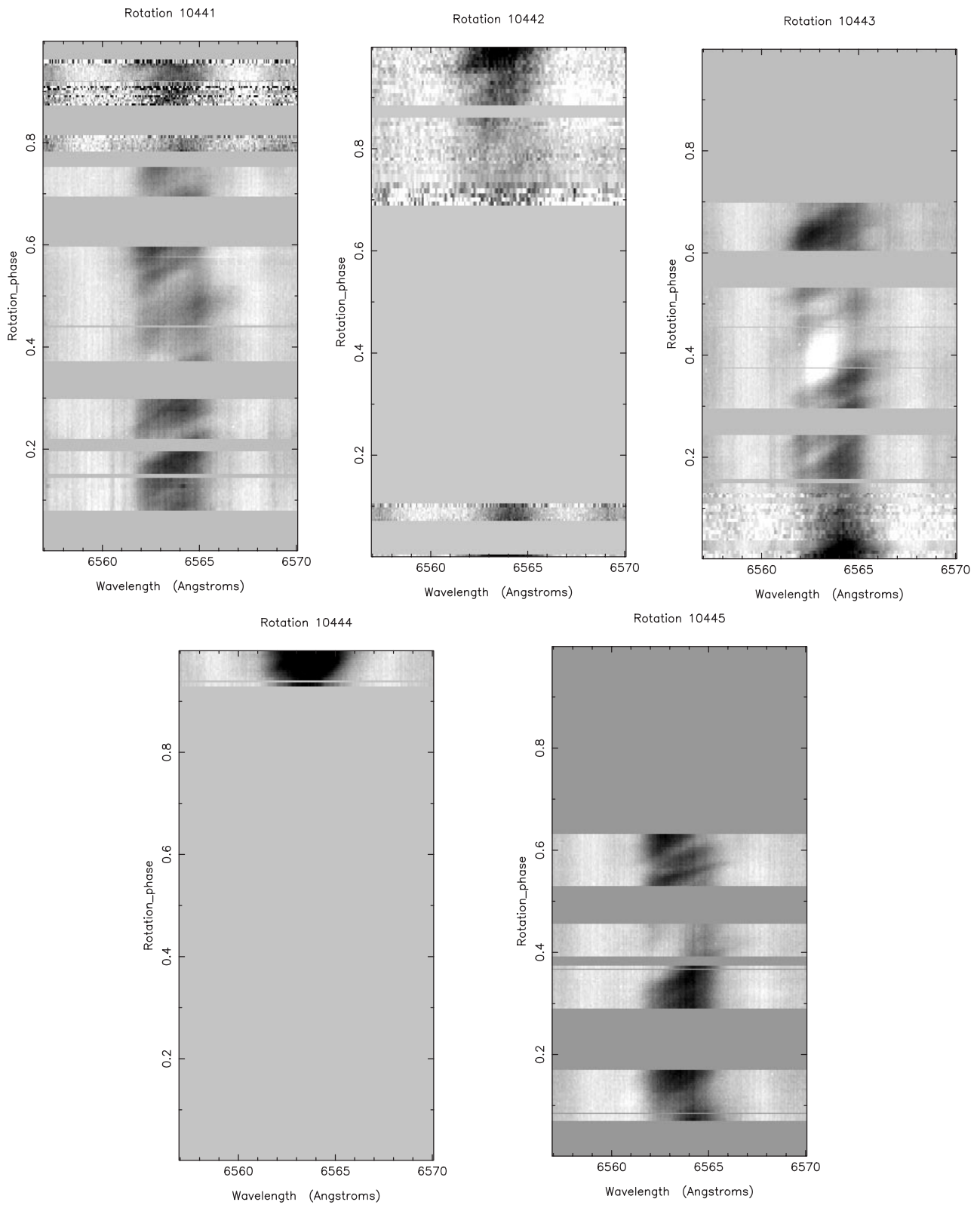


Figure 12. Phase-binned dynamic spectra of the H α profile in AB Dor observed at CTIO, SAAO and the AAT on the nights of 1995 November 15–17 UT. The rotation numbers and phases are derived from the ephemeris $HJD = 244\,4296.575 + 0.51479E$. The grey-scale runs from black at 0.80 times the local continuum level, to white at 1.02 times continuum.

Table 6. A list of transients observed repeatedly during the MUSICOS 1994 campaign, derived from the plots in Fig. 12. The three pairs of columns listing phase and axial distance refer to rotations 10441, 10443 and 10445 respectively. Uncertainties for axial distances are 95 per cent (2σ) confidence limits.

| Feature | Phase | ϖ/R_* | Phase | ϖ/R_* | Phase | ϖ/R_* |
|---------|-----------|---------------|-----------|-------------------|-----------|-------------------|
| A | 10441.00: | Present; gap | 10443.00: | Too diffuse | 10445.00: | Present; gap |
| B | 10441.19: | 3.1 ± 0.8 | 10443.19 | 3.1 ± 0.8 | 10445.19: | Present; gap |
| C | 10441.26: | Too diffuse | 10443.260 | 3.45 ± 0.12 | 10445.26: | Uncertain; gap |
| D | 10441.33: | Present; gap | 10443.330 | 4.85 ± 0.72 | 10445.340 | 3.33 ± 0.44 |
| E | 10441.46: | Too diffuse | 10443.48: | Faint; ~ 4.0 | 10445.48: | Uncertain; gap |
| F | – | – | – | – | 10445.550 | 7.96 ± 0.60 |
| G | 10441.557 | 3.0 ± 1.1 | 10443.56: | Present; gap | 10445.56: | Faint; ~ 3.5 |
| H | 10441.64: | Diffuse; gap. | 10443.64: | Too diffuse | 10445.64: | Diffuse; gap. |

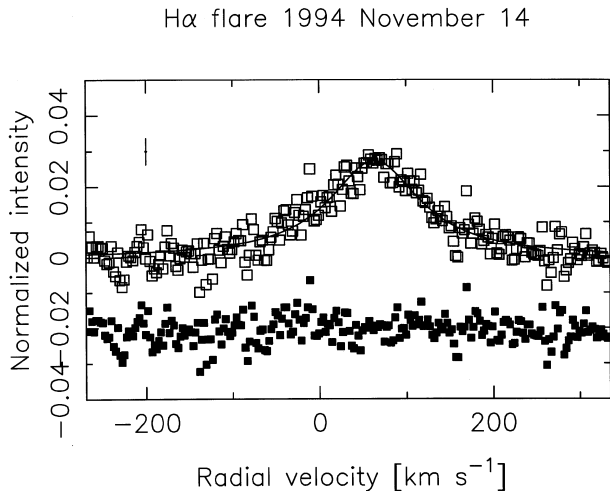


Figure 13. The H α profile of the flare observed at HJD 244 9671.793 (open squares), with the underlying stellar spectrum subtracted and a Lorentzian profile fitted as described in the text. The relative flux scale is in units of the local stellar continuum level, and the residuals from the fit are shown as filled squares. The rms error is shown as an error bar at top left.

were rebinned to a linear velocity scale with 2.5 km s^{-1} per bin. The signal to noise ratio per pixel in the rebinned spectra was approximately 20 in the blue wing of the Ca II H line. The spectra were normalized to unit average flux in the wavelength band from 396.500 to 396.575 nm. The resulting dynamic spectra for rotations 10443 and 10445 are illustrated in grey-scale form in Fig. 14.

The variations in the Ca II H emission profile are subtler than those seen in H α . In particular, at the relatively low signal to noise ratio of these observations, there are no obvious counterparts to the strong, rapidly moving absorption transients seen in H α around phases 0.3 and 0.55 to 0.65, although the overall emission strength does appear to be suppressed slightly at these phases.

There is, however, a sharply defined and slowly moving emission enhancement, which first appears at phase 10443.3, and drifts toward the red. The feature does not appear to be present in the data covering the same phase range in rotation 10445, and we conclude that this enhancement is probably associated with the flare seen in H α at phase 10443.4. To improve the contrast, we divided the dynamic spectra through by the time-averaged Ca II H profile from rotation 10445, in which no strong flares were seen. The residual profiles are shown in Fig. 15. The emission from the

flare clearly peaked just before phase 0.4. This is slightly earlier than the peak seen in H α but, as can be seen from Fig. 12, the early stages of the event appear to have been masked by an absorption transient in that line. The blue spectra clearly show He also to have been in emission during the flare.

During the decay phase of the flare, enhanced emission appears to be present in Ca II H and H ϵ until at least phase 0.6. It is possible that the brief increase in the emission strength seen near phase 0.55 could represent another flare event. This interpretation is, however, complicated by the passage of several cloud complexes across the stellar disc between phases 0.48 and 0.60. It is conceivable that the apparent drop in localized Ca II H emission around phase 0.50 could have been caused by the passage of one of these clouds across the line of sight to the flare site. The H α profile does not show any obvious renewal of flare emission at this phase, but it should be noted that there was a gap in the H α observations between phases 0.53 and 0.60, so no useful conclusion can be drawn.

7 DISCUSSION

The Doppler images confirm that starspot activity was present at all latitudes on the star, with the light curve modulation dominated by intermediate-latitude groups. A large and slightly asymmetric polar cap of spots was present. The spot activity in the polar regions has a filling factor and limiting lower latitude ($\sim 70^\circ$) similar to that seen in all our images obtained since 1992 January. The overall image morphology is similar to that observed in 1995 December by DC97, with activity present at nearly all latitudes.

Spots were found to be present in both hemispheres when broad-band photometry was used as an additional constraint on the reconstructed images. This serves to illustrate that simultaneous photometry is invaluable for resolving ‘mirror’ ambiguities about the equator. In the absence of photometry, the entropy constraint tends merely to change the sign of the latitude of any spot in the hemisphere turned away from the observer. The absolute value of the latitude is not affected, being constrained by the apparent radial acceleration of the spot feature in the line profiles. This being so, differential rotation studies based on spectroscopy alone will be unaffected by hemispheric ambiguities resulting from the lack of simultaneous broad-band photometry.

The 1994 November light curve of AB Doradus exhibited a range of magnitudes comparable with that reported by UCC95 for observations made with the same telescope a year previously. This suggests that no dramatic change in overall spot activity levels had taken place in the intervening year. Maximum light occurred between phase 0.8 and 1.0, and corresponds to the bright region seen in the Doppler images between longitudes 0° and 90° .

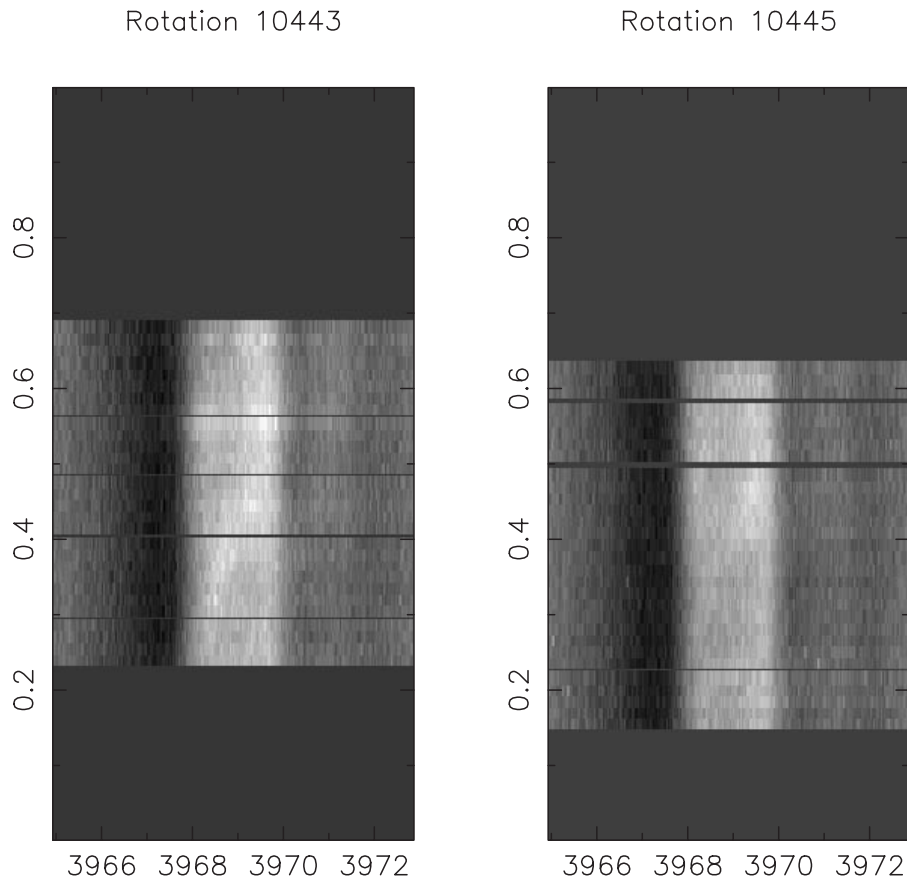


Figure 14. Phase-binned dynamic spectra of the Ca II H + He I profile in AB Dor observed at the ESO CAT/CES on the nights of 1995 November 16–17 UT. The rotation numbers and phases are derived from the ephemeris $HJD = 244\,4296.575 + 0.51479E$. The grey-scale runs from black at 0.44 times the mean flux level across the profile, to white at 1.67 times the mean level.

Although this was the most poorly sampled part of the rotation cycle, inspection of Figs 4 to 6 confirms that no strong starspot features seem to be present in this phase interval, at least at the intermediate latitudes that have the strongest influence on the light curve.

While the two-day span of the spectroscopic observations is not sufficient to justify a full differential rotation determination, it is worth noting that the ESO *VRI* photometry was continued for several nights beyond the end of the CTIO run. During this time, small but significant changes to the light curve morphology are apparent from Fig. 2. Most of these occur near maximum light. The descending branch of the light curve is, however, well observed throughout the run, and shows no significant phase drift. Bos et al. (1996), however, have published a light curve secured mainly between 1994 November 25 and 28. This light curve has similar morphology to ours, but the minimum is clearly centred at phase 0.45. This implies a drift of 0.05 ± 0.01 rotations toward earlier phases in the intervening 9 days. The rotation period of the spot complex responsible for the photometric minimum is therefore in the range 0.5133 ± 0.0003 d. This suggests that the main photometric signal must arise at latitudes whose rotation rate corresponds closely to this period. The differential rotation law determined by DC97, in which

$$\Omega(l) = 12.2434 - 0.0564 \sin^2 l \text{ rad d}^{-1},$$

then indicates that the spot complex must lie at an average latitude of 15° or so, with an uncertainty extending from the equator to latitude 25° . This corresponds closely to the latitude of the spot complex between longitudes 120° and 190° in all the reconstructed images.

A high level of circumstellar prominence activity was present throughout the run. Eight major prominence complexes were identified and tracked throughout the run to the extent permitted by gaps in the observations. Significant evolution of the prominence system was apparent over the four stellar rotations covered. In particular, one feature was seen to move out to a distance of 8 stellar radii from the stellar rotation axis on the last night of the CTIO run. If our tentative identification of the precursor to this event is correct, a cloud initially located at about 3 or 4 stellar radii from the rotation axis moved away from the star, progressively lagging further in phase as it moved outward.

Short-duration flare activity was observed in the *U* band, in the Ca II H + He I lines, and in H α on several occasions. There is no obvious correlation between either the surface spots or the flare activity and the system of circumstellar prominences. It is clear that AB Dor itself, rather than the dMe-star visual companion Rst 137B, is the origin of most of the *U*-band flare activity observed both by Rucinski (1995) and by ourselves. In Rucinski's case, the identification of the flaring star is made possible by his use of CCD imaging as opposed to single-channel photometry. The flares appear to consist of two main types. Brief *U*-band outbursts, with

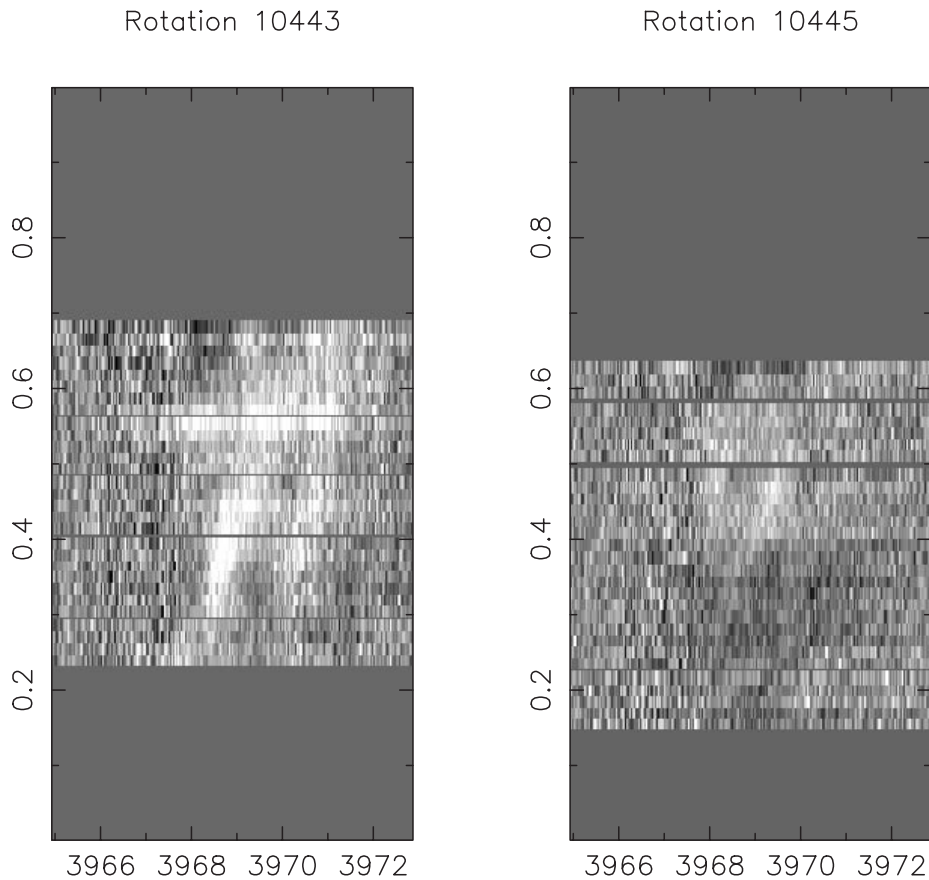


Figure 15. Phase-binned dynamic spectra of the Ca II H + He I profile in AB Dor observed at the ESO CAT/CES on the nights of 1995 November 16–17 UT. The rotation numbers and phases are derived from the ephemeris $HJD = 244\,4296.575 + 0.51479E$. The mean spectrum on the night of 1994 November 17 has been divided out, and the grey-scale runs from black at 0.95 times the mean level of the residual spectrum, to white at 1.05 times the mean level.

U -band amplitudes of no more than 0.03 mag or so, are seen to last no more than a minute or two, and are accompanied in at least one instance by a short-lived, broad emission enhancement in $H\alpha$. Indeed, the association of the $H\alpha$ enhancement with one of these U -band flares confirms that AB Dor was indeed the site of the flare.

One longer duration flare was also observed in $H\alpha$ and in the Ca II H + He I lines, with mid-event at phase 10443.40. There is some evidence in the V -band light curves on this and the following night, that this flare may have had a significant optical-continuum counterpart. Comparison of the V -band light curve in Fig. 2(a) for rotations 10443 (filled triangles) and 10445 (open triangles) reveals a considerably greater discrepancy than can readily be explained by differential rotation over the course of 24 hours. The two light curves diverge shortly after phase 0.30, and appear not to converge again until at least phase 0.50. Throughout this 3-h period, the V magnitude of the star was consistently 0.02 mag brighter during rotation 10443 than at the corresponding phases during rotation 10445. It is notable that this V -band enhancement coincides precisely with the time interval in which the long-duration flare was seen in $H\alpha$ and Ca II H. For an assumed distance of 15 pc and $V \approx 6.93$, the total energy radiated in the V band by a 0.02-mag flare over the observed 3-h duration of the optical enhancement, is of order 1 to 2×10^{34} erg. Interestingly, the enhancement in the U -band magnitude of AB Dor at this time is no more than that in V . A second long-duration flare was also

seen in the broad-band photometry following the end of the spectroscopic run. While the energy released in this flare was comparable with the November 15/16 event, the optical signature was seen to be much stronger in the U band than at longer wavelengths.

In both long-duration flares, our estimates of the total optical energy released are comparable to the total 0.1 to 10 keV X-ray energy released in the long-duration X-ray flares observed in 1984 December and 1986 January by Collier Cameron et al. (1988) using the *EXOSAT* spacecraft (after allowance is made for the fact that in that paper the distance of AB Dor was assumed to be 20 rather than 15 pc). These flares were characterized by soft X-ray rise times of order 2 h, during which the emission measure rose steadily at almost constant temperature, as though a loop with a length of several stellar radii were being steadily filled with plasma ablated off the photosphere or chromosphere. We suspect that the long-duration optical flares seen here may well be the optical counterpart of the same kind of flare. The present observations suggest strongly that particle acceleration at the flare site can persist for 2 to 3 h in such flares, heating the chromosphere sufficiently to produce the observed $H\alpha$ and Ca II H emission, with some fraction of the particles being thermalized deep enough in the photosphere to give the observed V -band enhancement. A similar explanation, attributed to an idea by Ambartsumian (1957), was advanced by Haro (1968) as an explanation for the dichotomy between long-duration red-continuum

flares and short-duration UV flares observed among flare stars in the Orion region. Haro noted further that although relatively few stars were seen to exhibit these ‘slow’ flares, the majority among these had also been seen to undergo more conventional short-duration flaring. Taken together with recently published observations of a comparably long optical flare on LQ Hya (Montes et al. 1999), these observations suggest that long-duration optical and X-ray flares of this kind are a fairly frequent occurrence on single stars as well as on RS CVn binaries such as HR 1099. This argues against a flare energy storage/release mechanism that relies solely on the binary nature of the RS CVn systems.

It is tempting to speculate that there could be a physical association between the escaping cloud seen on the last night of the CTIO run, and the long-duration flare observed on 1994 November 15/16. We note that the phase at which the precursor cloud was initially located corresponds closely to the phase at which the Ca II H signature of the 1994 November 15/16 flare crossed the centre of the disc. The release of magnetic stresses in the confining loop structure of a cloud undergoing centrifugal ejection could conceivably result in an extended period of particle acceleration and consequent bombardment of the photosphere and chromosphere beneath the rising cloud. It would also provide naturally the long loop structures needed to explain the long rise times and near-constant plasma temperatures of the long-duration soft X-ray flares observed by Collier Cameron et al. (1988) in this same star. The release of these stresses would then allow the cloud to begin to move outward. If the magnetic torques exerted by the expanding loop are insufficient to maintain strict corotation, the cloud will lag the rotation of the star as it moves outward.

ACKNOWLEDGMENTS

We are saddened to report the untimely death of our co-author Professor Zhai Disheng in the time since this work was completed. Professor Zhai was one of the founding members of the MUSICOS collaboration, and his scientific insights and good humour will be sadly missed. We dedicate this paper to his memory. We thank Brad Carter for bringing Haro’s early work on slow flares to our attention, and an anonymous referee for numerous helpful criticisms of the original manuscript. This paper was based on observations obtained at Cerro Tololo Inter-American Observatory, the South African Astronomical Observatory, the Anglo-Australian Telescope and the European Southern Observatory.

REFERENCES

- Ambartsumian V., 1957, in Herbig G. H., ed., Proc. IAU Symp. 3, Non-stable Stars. Cambridge Univ. Press, London, p. 177
- Balona L. A. et al., 1996, MNRAS, 281, 1315
- Baudrand J., Böhm T., 1992, A&A, 259, 711
- Böhm T. et al., 1996, A&AS, 120, 431
- Bos M., Budding E., Hudson G., Hudson R., 1996, Inf. Bull. Variable Stars No. 4203
- Catala C. et al., 1993, A&A, 275, 245
- Catala C., Boehm T., Donati J. F., Simon T., Jiang S., Zhao F., 1997, A&A, 319, 176
- Collier Cameron A., 1995, MNRAS, 275, 534 (C95)
- Collier Cameron A., 1997, MNRAS, 287, 556
- Collier Cameron A., Robinson R. D., 1989a, MNRAS, 236, 57
- Collier Cameron A., Robinson R. D., 1989b, MNRAS, 236, 657
- Collier Cameron A., Unruh Y. C., 1994, MNRAS, 269, 814 (CU94)
- Collier Cameron A., Bedford D. K., Rucinski S. M., Vilhu O., White N. E., 1988, MNRAS, 231, 131
- Collier Cameron A., Jeffery C. S., Unruh Y. C., 1992, in Jeffery C. S., Griffin R. E., eds, Stellar Chromospheres, Coronae and Winds. Institute of Astronomy, Cambridge, p. 81
- Diego F., Walker D. D., 1985, MNRAS, 217, 347
- Donati J.-F., Collier Cameron A., 1997, MNRAS, 291, 1 (DC97)
- Donati J. F., Semel M., Carter B., Rees D. E., Collier Cameron A., 1997, MNRAS, 291, 658
- Donati J. F., Collier Cameron A., Hussain G. A. J., Semel M., 1999, MNRAS, 302, 437
- Foing B. H. et al., 1994, A&A, 292, 543
- Haro G., 1968, Flare stars. Univ. Chicago Press, Chicago & London, p. 141
- Hubert A. et al., 1997, A&A, 324, 929
- Innis J. L., Thompson K., Coates D. W., Lloyd Evans T., 1988, MNRAS, 235, 1411
- Kennelly E. et al., 1996, A&A, 313, 571
- Kürster M., Schmitt J. H. M. M., Cutispoto G., 1994, A&A, 289, 899
- Kurucz R. L., 1993, Technical Report, Harvard-Smithsonian Center for Astrophysics, Cambridge, MA
- Mills D., 1994, Starlink User Note 152, Rutherford Appleton Laboratory
- Montes D., Saar S., Collier Cameron A., Unruh Y. C., 1999, MNRAS, 305, 45
- Rucinski S. M., 1995, Inf. Bull. Variable Stars No. 4156
- Skilling J., Bryan R. K., 1984, MNRAS, 211, 111
- Unruh Y. C., Collier Cameron A., 1995, MNRAS, 273, 1
- Unruh Y. C., Collier Cameron A., Cutispoto G., 1995, MNRAS, 277, 1145 (UGC95)
- Vilhu O., Muhli P., Huovelin J., Hakala P., Rucinski S. M., Collier Cameron A., 1998, AJ, 115, 1610
- Zhai D. S., Foing B. H., Cutispoto G., Zhang R. X., Catala C., Char S., Zhang X. B., Jankov S., 1994, A&A, 282, 168

This paper has been typeset from a $\text{\TeX}/\text{\LaTeX}$ file prepared by the author.